Composite Structures 157 (2016) 483–493

Contents lists available at ScienceDirect

Composite Structures

journal homepage: www.elsevier.com/locate/compstruct

Vibrational and acoustic responses of a laminated plate with temperature gradient along the thickness

Meng Du, Qian Geng, Yue-ming Li *

State Key Laboratory for Strength and Vibration of Mechanical Structures, Shaanxi Key Laboratory of Environment and Control for Flight Vehicle, School of Aerospace Engineering, Xi'an Jiaotong University, Xi'an 710049, People's Republic of China

ARTICLE INFO

Article history:
Available online 19 January 2016

Keywords:
Laminated plates
Vibration
Acoustic response
Temperature gradient

ABSTRACT

Analytical study is carried out on the dynamic characteristics of a laminated plate under temperature gradient. Theoretical formulations are derived with the first order shear deformation theory and von Karman nonlinear strain displacement relationship considering the effect of temperature gradient. Semi-analytical solutions of vibration and acoustic responses are obtained for different temperature gradients. The correctness of the theoretical method is demonstrated by comparing with the experimental result and numerical simulation. The present work theoretically explains why the lowest point (buckling occurring) of the experimental curve of resonant frequencies for thermal structure is shifting up away from the horizontal axis. It also means that initial thermal deformation and thermal stress have to be considered together in simulation of the dynamical response for thermal structure. Research results show that with increasing temperature gradients, the resonant frequency increases, the critical mid-plane temperature at which resonant frequency drops to the lowest decreases, and the response peaks move toward higher frequency.

1. Introduction

Hypersonic spacecrafts suffer harsh aerodynamic heating in service. Local high temperature gradient would give rise to non-uniform thermal stress, even local thermal buckling. Thermal environment would result in changing of the stiffness and dynamic response of structures. Therefore, it's significant to research the dynamic characteristics of the thermal structures.

The laminated plate is a typical structure of spacecrafts, of which vibrational and acoustic responses in thermal environment were studied by many researchers. Jeyaraj et al. [1,2] presented numerical simulation studies on vibrational and acoustic responses of rectangular plates in thermal environment considering the inherent material damping property. The critical buckling temperatures and vibrational responses were obtained using finite element method while sound radiation responses were obtained using a coupled FEM/BEM technique. Yang and Shen [3,4] analyzed the free vibration with shear and normal deformations effects and forced vibration for initially stressed functionally graded plates in thermal environments. In their study, the temperature dependence of material properties were considered. Pradeep et al. [5,6] studied free vibration and critical buckling temperature of the viscoelastic sandwich plates taking the temperature dependence of properties and effects of pre-stresses into account using finite element method. Geng et al. [7–9] investigated the influence of thermal environments on vibrational and acoustic responses of rectangular thin plates with simply supported and clamped boundary conditions through the theoretical analysis, numerical simulation and experimental method, and the results obtained by three methods agree well with each other. Based on the equivalent non-classical theory, Liu and Li [10] derived analytical solutions of the vibrational and acoustic responses for a rectangular sandwich plate under thermal environments. The influences caused by thermal environment on the sandwich and the specific features of various sandwich plates are deeply discussed in their study. Li and Li [11] carried out analytical studies on the vibration and sound radiation characteristics for a rectangular laminated plate taking the effect of thermal environment into account. Applying the piecewise low order shear deformation theory, Li and Yu [12] investigated the vibration and acoustic responses of the sandwich panels constituted of orthotropic materials applied a concentrated harmonic force in a high temperature environment. Zhang et al. [13] researched a sandwich structure composed of fiber-reinforced mullite matrix composite face sheets and ceramic foams elastic layer subjected to high temperature and large gradient

* Corresponding author.
E-mail address: liyueming@mail.xjtu.edu.cn (Y.-m. Li).

http://dx.doi.org/10.1016/j.compstruct.2016.01.063
0263-8223/

thermal environment by both experimental means and finite element method. The influence of the plate geometry, the geometry of the cut-out, the moisture concentration, the thermal gradient and the boundary conditions on the free flexural vibration and buckling of laminated composite plates were numerically studied within the framework of the extended finite element method by Natarajan et al. [14,15]. Rath et al. [16,17] carried out both experimental and numerical investigation on the free vibration behavior of laminated composite plates subjected to varying temperature and moisture.

A few researchers studied the effects of temperature gradient on the vibration of laminated plates. The dynamic free response of thin rectangular plates subjected to one and two dimensional steady state temperature distributions satisfying Laplace's equation was investigated by using the finite difference method and finite element method [18,19]. Gupta [20] analyzed the vibration of non-homogenous viscoelastic rectangular plates of linearly varying thickness subjected to thermal gradient. The effect of a constant thermal gradient on the transverse vibrational frequencies of a simply supported rectangular plate was investigated by Fauconneau and Marangoni [21] with various plate width-to-length ratios as functions of a parameter related to the temperature dependence of the elastic modulus of the material. Chen et al. [22] presented a study on the buckling and vibration of initially stressed composite plates with temperature-dependent material properties in thermal environments. In Refs. [21,22], the effect of thermal gradient was considered by temperature-dependent material properties. The above researches on laminated plates are all based on the linear theory. With the nonlinear effect, the researches on thermal post-buckled and large amplitude vibration were presented in a number of literatures. Based on a higher-order shear deformation theory incorporating von-Karman nonlinear strain–displacement relations, Girish and Ramachandra [23] analyzed the post-buckled vibration of a symmetrically laminated composite plate subjected to a uniform temperature distribution through the thickness numerically. Park and Kim [24] investigated thermal post-buckling and vibration behaviors of the functionally graded plate by nonlinear finite element method. A closed form solution for linear and nonlinear free vibrations of composite and fiber metal laminated rectangular plates was obtained with the multiple time scales method by Shooshtari and Razavi [25]. Amabili [26,27] investigated large-amplitude vibrations of rectangular plates subjected to harmonic excitations, and the results were compared considering different boundary conditions by theory and experiment methods. Bhimaraddi and Chandrashekhara [28] analyzed the large amplitude vibrations, buckling and post-buckling of heated angle-ply laminated plates using the parabolic shear deformation theory, and the effects of initial imperfections and the temperature loading on the response characteristics of the plate were discussed. Chen et al. [29] derived the nonlinear partial differential equations for the vibrating motion of a plate based on a modified plate theory, and studied the large amplitude vibrations of an initial stressed plate. Shen and Huang [30,31] presented the nonlinear vibration and dynamic response of functionally graded material plates in thermal environments. The results revealed that the temperature field and volume fraction distribution have a significant effect on the nonlinear vibration and dynamic response of the functionally graded plate. Murphy et al. [32] investigated the effect of thermal pre-stress on the free vibration characteristics of clamped rectangular plates in a combined theoretical and experiment approach. The effect of initial geometric imperfections, modal coupling, imperfect clamping and post-buckling were addressed.

Li et al. [33,34] carried out a computational analysis of the nonlinear vibration and thermal post-buckling of a heated orthotropic annular plate with a central rigid mass for the cases of immovably hinged as well as clamped constraint conditions of the outer edge.

In previous studies, researchers mostly focus on temperature-dependent material properties. It is well known that Young's modulus is a certain function of temperature, by which the effect of temperature is considered. The research on this aspect is mature and the research method is visual. Therefore, this article pays no attention to the temperature dependent material properties, but focuses on the effect of thermal stress and thermal deformation. Effect of thermal stress is also researched in a few literatures as the above. However, none of available researches are found on dynamical characteristics of laminated plates considering the effect of thermal deformation due to thermal gradient. The present work conducts the theoretical research on vibro-acoustic characteristics of a laminated plate with temperature gradient along the thickness direction. The vibration governing equations are established considering the initial deflection caused by temperature gradient. Vibrational and acoustic responses are analyzed theoretically with varying temperature gradients. The experimental result and numerical simulation are used for validation, and both show good agreements with present solutions.

2. Formulate

We consider an n-layer laminated plate as shown in Fig. 1(a). The mid-plane of laminated plate is lying on the x–y plane. Based on the first-order shear deformation theory, displacement fields are expressed as

$$\begin{aligned} u(x,y,z,t) &= u^0(x,y,t) + z\varphi_x(x,y,t) \\ v(x,y,z,t) &= v^0(x,y,t) + z\varphi_y(x,y,t) \\ w(x,y,z,t) &= w^0(x,y,t) \end{aligned} \tag{1}$$

where u, v, and w are the in-plane displacements and the transverse displacement at any point along x, y, z, directions, respectively. u^0, v^0, w^0 are the corresponding displacements of the point on the mid-plane, φ_x and φ_y are the rotations of a transverse normal about the y-axes and x-axes, respectively.

It is assumed that the laminated plate is subjected to the linear temperature distribution along the thickness direction as shown in Fig. 1(b),

$$\Delta T = T_0 + \tau z \tag{2}$$

where T_0 and τ are the temperature rise at mid-plane and temperature gradient along the thickness, respectively.

In this paper, arbitrary temperature distribution can be divided into two parts. One is mid-plane temperature distribution which causes expansion and contraction at mid-plane, the other is temperature gradient along the thickness which induces thermal bending deformation. The effects of temperature in plane on the expansion and compression have been studied very much in Refs. [7–11,35]. So, the present study focuses on the effects of thermal bending deformation caused by temperature gradient on vibrational and acoustic characteristics. Assuming the initial thermal deformations induced by temperature gradient (or thermal post-buckling) are $u_s^0(x,y)$, $v_s^0(x,y)$, $w_s^0(x,y)$, $\varphi_{xs}(x,y)$, $\varphi_{ys}(x,y)$, the total displacements should be expressed as

$$\begin{aligned} u^0(x,y,t) &= u_s^0(x,y) + u_t^0(x,y,t) \\ v^0(x,y,t) &= v_s^0(x,y) + v_t^0(x,y,t) \\ w^0(x,y,t) &= w_s^0(x,y) + w_t^0(x,y,t) \\ \varphi_x(x,y,t) &= \varphi_{xs}(x,y) + \varphi_{xt}(x,y,t) \\ \varphi_y(x,y,t) &= \varphi_{ys}(x,y) + \varphi_{yt}(x,y,t) \end{aligned} \tag{3}$$

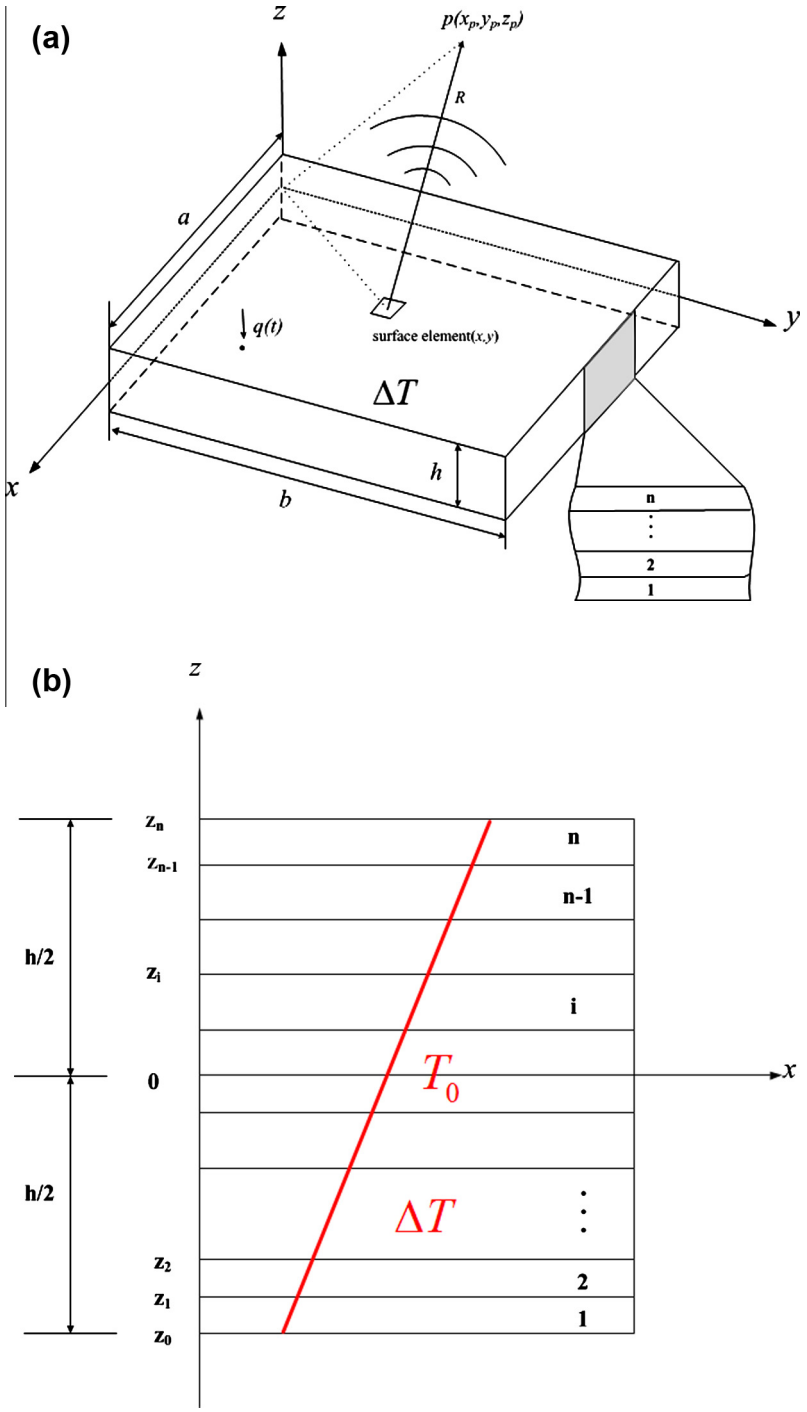

Fig. 1. Laminated plate model, (a) global view, (b) cross view.

where the characters with the subscripts '*s*' are the initial static deformation due to temperature gradient (or thermal post-buckling), and the characters with the subscripts '*t*' are the dynamical deformation caused by vibration of the structures.

For considering the initial deflections, von-Karman nonlinear strain–displacement relation is adopted as follows:

$$\begin{aligned} &\varepsilon_{xx} = \varepsilon^0_{xx} + z\chi_{xx}, \quad \varepsilon_{yy} = \varepsilon^0_{yy} + z\chi_{yy}, \quad \varepsilon_{zz} = 0 \\ &\varepsilon_{xy} = \varepsilon^0_{xy} + z\chi_{xy}, \quad \varepsilon_{yz} = \varepsilon^0_{yz}, \quad \varepsilon_{xz} = \varepsilon^0_{xz} \end{aligned} \tag{4}$$

where

$$\begin{aligned} &\varepsilon^0_{xx} = \frac{\partial u^0}{\partial x} + \frac{1}{2}\left(\frac{\partial w^0}{\partial x}\right)^2, \quad \varepsilon^0_{yy} = \frac{\partial v^0}{\partial y} + \frac{1}{2}\left(\frac{\partial w^0}{\partial y}\right)^2, \\ &\varepsilon^0_{xy} = \frac{\partial u^0}{\partial y} + \frac{\partial v^0}{\partial x} + \frac{\partial w^0}{\partial x}\frac{\partial w^0}{\partial y}, \\ &\varepsilon^0_{yz} = \frac{\partial w^0}{\partial y} + \varphi_y, \quad \varepsilon^0_{xz} = \frac{\partial w^0}{\partial x} + \varphi_x, \quad \chi_{xx} = \frac{\partial \varphi_x}{\partial x}, \\ &\chi_{yy} = \frac{\partial \varphi_y}{\partial y}, \quad \chi_{xy} = \frac{\partial \varphi_x}{\partial y} + \frac{\partial \varphi_y}{\partial x} \end{aligned} \tag{5}$$

With the effect of temperature gradient, the constitutive relations for a laminated plate made up of n layers of orthotropic plates may be written in the following form:

$$\begin{bmatrix}\sigma_{xx}\\ \sigma_{yy}\\ \sigma_{xy}\\ \sigma_{yz}\\ \sigma_{xz}\end{bmatrix}=\begin{bmatrix}\sigma^0_{xx}\\ \sigma^0_{yy}\\ \sigma^0_{xy}\\ \sigma^0_{yz}\\ \sigma^0_{xz}\end{bmatrix}+\begin{bmatrix}\sigma^T_{xx}\\ \sigma^T_{yy}\\ \sigma^T_{xy}\\ \sigma^T_{yz}\\ \sigma^T_{xz}\end{bmatrix}=\begin{bmatrix}C_{11} & C_{12} & 0 & 0 & 0\\ C_{21} & C_{22} & 0 & 0 & 0\\ 0 & 0 & C_{66} & 0 & 0\\ 0 & 0 & 0 & C_{44} & 0\\ 0 & 0 & 0 & 0 & C_{55}\end{bmatrix}\times\begin{bmatrix}\varepsilon_{xx}\\ \varepsilon_{yy}\\ \varepsilon_{xy}\\ \varepsilon_{yz}\\ \varepsilon_{xz}\end{bmatrix}+\begin{bmatrix}C_{11} & C_{12} & 0 & 0 & 0\\ C_{21} & C_{22} & 0 & 0 & 0\\ 0 & 0 & C_{66} & 0 & 0\\ 0 & 0 & 0 & C_{44} & 0\\ 0 & 0 & 0 & 0 & C_{55}\end{bmatrix}\times\begin{bmatrix}-\alpha_{xx}\Delta T\\ -\alpha_{yy}\Delta T\\ -\alpha_{xy}\Delta T\\ 0\\ 0\end{bmatrix} \tag{6}$$

where σ^0_{ij} and σ^T_{ij} are mechanical stresses and thermal stresses respectively; C_{ij} are the material stiffness of laminated plates; α_{ij} are thermal expansion coefficient.

Hamilton's principle is applied to derive the governing equations

$$\int \delta(U-T+V)dt=0 \tag{7}$$

Here δ is the variation of the functions. U, T and V are the strain energy, the kinetic energy, work due to external force, which can be written as

$$\begin{aligned}U&=\frac{1}{2}\int\int\int\sigma_{ij}\varepsilon_{ij}dxdydz\\ T&=\frac{1}{2}\int\int\int\rho\left[\left(\frac{\partial\mu}{\partial t}\right)^2+\left(\frac{\partial v}{\partial t}\right)^2+\left(\frac{\partial w}{\partial t}\right)^2\right]dxdydz\\ V&=\int\int qwdxdy\end{aligned} \tag{8}$$

in which q is applied force.

Substituting the integral forms of U, T and V into Eq. (7), performing the variation and integral, the governing equations can be obtained.

For a symmetric laminated plate, there is no bending-extensional coupling stiffness, that is B_{ij} $(i,j=1,2,6)=0$, then the governing equations are simplified as

$$\begin{aligned}&A_{11}u^0_{,xx}+A_{66}u^0_{,yy}+(A_{12}+A_{66})v^0_{,xy}+w^0_{,x}(A_{11}w^0_{,xx}+A_{66}w^0_{,yy})\\ &+(A_{12}+A_{66})w^0_{,y}w^0_{,xy}-\left(N^T_{xx,x}+N^T_{xy,y}\right)=R_0u^0_{,tt}(A_{12}+A_{66})u^0_{,xy}\\ &+A_{66}v^0_{,xx}+A_{22}v^0_{,yy}+(A_{12}+A_{66})w^0_{,x}w^0_{,xy}+w^0_{,y}\left(A_{66}w^0_{,xx}+A_{22}w^0_{,yy}\right)\\ &-\left(N^T_{yy,y}+N^T_{xy,x}\right)=R_0v^0_{,tt}w^0_{,x}\\ &\begin{pmatrix}A_{11}u^0_{,xx}+A_{66}u^0_{,yy}+(A_{12}+A_{66})v^0_{,xy}+w^0_{,x}\left(A_{11}w^0_{,xx}+A_{66}w^0_{,yy}\right)+\\ (A_{12}+A_{66})w^0_{,y}w^0_{,xy}-\left(N^T_{xx,x}+N^T_{xy,y}\right)\end{pmatrix}\\ &+w^0_{,y}\begin{pmatrix}(A_{12}+A_{66})u^0_{,xy}+A_{66}v^0_{,xx}+A_{22}v^0_{,yy}+(A_{12}+A_{66})w^0_{,x}w^0_{,xy}+\\ w^0_{,y}\left(A_{66}w^0_{,xx}+A_{22}w^0_{,yy}\right)-\left(N^T_{yy,y}+N^T_{xy,x}\right)\end{pmatrix}\\ &+w^0_{,xx}\left(A_{11}\left(u^0_{,x}+\frac{1}{2}(w^0_{,x})^2\right)+A_{12}\left(v^0_{,y}+\frac{1}{2}(w^0_{,y})^2\right)-N^T_{xx}\right)\\ &+w^0_{,yy}\left(A_{12}\left(u^0_{,x}+\frac{1}{2}(w^0_{,x})^2\right)+A_{22}\left(v^0_{,y}+\frac{1}{2}(w^0_{,y})^2\right)-N^T_{yy}\right)\\ &+2w^0_{,xy}\left(A_{66}\left(u^0_{,y}+v^0_{,x}+w^0_{,x}w^0_{,y}\right)-N^T_{xy}\right)+A_{55}\left(w^0_{,xx}+\varphi_{x,x}\right)\\ &+A_{44}(w^0_{,yy}+\varphi_{y,y})+q=R_0w^0_{,tt}D_{11}\varphi_{x,xx}+D_{12}\varphi_{y,xy}+D_{66}\varphi_{x,xy}\\ &+D_{66}\varphi_{y,xy}-A_{55}w^0_{,x}-A_{55}\varphi_x-\left(M^T_{xx,x}+M^T_{xy,y}\right)=R_2\varphi_{x,tt}D_{66}\varphi_{x,xy}\\ &+D_{66}\varphi_{y,xx}+D_{21}\varphi_{x,xy}+D_{22}\varphi_{y,yy}-A_{44}w^0_{,y}-A_{44}\varphi_y\\ &-\left(M^T_{yy,y}+M^T_{xy,x}\right)=R_2\varphi_{y,tt}\end{aligned} \tag{9}$$

where A_{ij}, D_{ij} $(i,j=1,2,6)$ are the coefficients of extensional and bending stiffness, respectively. A_{44} and A_{55} are the shear stiffness coefficients. Thermal stress resultants N^T_{xx}, N^T_{yy}, N^T_{xy} and moment resultants M^T_{xx}, M^T_{yy}, M^T_{xy} are included in the governing equations. These coefficients associated with material parameters and thermal stresses are defined as follows:

$$\begin{aligned}(A_{ij},D_{ij})&=\int_{-h/2}^{h/2}C_{ij}(1,z^2)dz\quad(i,j=1,2,4,5,6)\\ (R_0,R_2)&=\int_{-h/2}^{h/2}\rho(1,z^2)dz\\ \left(N^T_{ij},M^T_{ij}\right)&=\int_{-h/2}^{h/2}\sigma^T_{ij}(1,z)dz\quad(i,j=x,y)\end{aligned} \tag{10}$$

It is assumed that the boundary conditions are all four edges clamped as follows

$$\begin{aligned}u^0=v^0=w^0=\varphi_x=\varphi_y=\frac{\partial w^0}{\partial x}=0\quad\text{at}\quad x=0,\ a\\ u^0=v^0=w^0=\varphi_x=\varphi_y=\frac{\partial w^0}{\partial y}=0\quad\text{at}\quad y=0,\ b\end{aligned} \tag{11}$$

Firstly, the thermal bending deformations $u^0_s(x,y)$, $v^0_s(x,y)$, $w^0_s(x,y)$, $\varphi_{xs}(x,y)$, $\varphi_{ys}(x,y)$ due to temperature gradient (or thermal post-buckling) in Eq. (3) are solved. Substituting $u^0_s(x,y)$, $v^0_s(x,y)$, $w^0_s(x,y)$, $\varphi_{xs}(x,y)$, $\varphi_{ys}(x,y)$ into Eq. (9), we can obtain the following static equations

$$\begin{aligned}&A_{11}u^0_{s,xx}+A_{66}u^0_{s,yy}+(A_{12}+A_{66})v^0_{s,xy}+w^0_{s,x}\left(A_{11}w^0_{s,xx}+A_{66}w^0_{s,yy}\right)\\ &+(A_{12}+A_{66})w^0_{s,y}w^0_{s,xy}-\left(N^T_{xx,x}+N^T_{xy,y}\right)=0(A_{12}+A_{66})u^0_{s,xy}\\ &+A_{66}v^0_{s,xx}+A_{22}v^0_{s,yy}+(A_{12}+A_{66})w^0_{s,x}w^0_{s,xy}\\ &+w^0_{s,y}\left(A_{66}w^0_{s,xx}+A_{22}w^0_{s,yy}\right)-\left(N^T_{yy,y}+N^T_{xy,x}\right)\\ &=0w^0_{s,x}\begin{pmatrix}A_{11}u^0_{s,xx}+A_{66}u^0_{s,yy}+(A_{12}+A_{66})v^0_{s,xy}+w^0_{s,x}\left(A_{11}w^0_{s,xx}+A_{66}w^0_{s,yy}\right)+\\ (A_{12}+A_{66})w^0_{s,y}w^0_{s,xy}-\left(N^T_{xx,x}+N^T_{xy,y}\right)\end{pmatrix}\\ &+w^0_{s,y}\begin{pmatrix}(A_{12}+A_{66})u^0_{s,xy}+A_{66}v^0_{s,xx}+A_{22}v^0_{s,yy}+(A_{12}+A_{66})w^0_{s,x}w^0_{s,xy}+\\ w^0_{s,y}\left(A_{66}w^0_{s,xx}+A_{22}w^0_{s,yy}\right)-\left(N^T_{yy,y}+N^T_{xy,x}\right)\end{pmatrix}\\ &+w^0_{s,xx}\left(A_{11}\left(u^0_{s,x}+\frac{1}{2}(w^0_{s,x})^2\right)+A_{12}\left(v^0_{s,y}+\frac{1}{2}(w^0_{s,y})^2\right)-N^T_{xx}\right)\\ &+w^0_{s,yy}\left(A_{12}\left(u^0_{s,x}+\frac{1}{2}(w^0_{s,x})^2\right)+A_{22}\left(v^0_{s,y}+\frac{1}{2}(w^0_{s,y})^2\right)-N^T_{yy}\right)\\ &+2w^0_{s,xy}\left(A_{66}\left(u^0_{s,y}+v^0_{s,x}+w^0_{s,x}w^0_{s,y}\right)-N^T_{xy}\right)+A_{55}\left(w^0_{s,xx}+\varphi_{sx,x}\right)\\ &+A_{44}\left(w^0_{s,yy}+\varphi_{sy,y}\right)=0D_{11}\varphi_{sx,xx}+D_{12}\varphi_{sy,xy}+D_{66}\varphi_{sx,yy}+D_{66}\varphi_{sy,xy}\\ &-A_{55}w^0_{s,x}-A_{55}\varphi_{sx}-\left(M^T_{xx,x}+M^T_{xy,y}\right)=0D_{66}\varphi_{sx,xy}+D_{66}\varphi_{sy,xx}+D_{21}\varphi_{sx,xy}\\ &+D_{22}\varphi_{sy,yy}-A_{44}w^0_{s,y}-A_{44}\varphi_{sy}-\left(M^T_{yy,y}+M^T_{xy,x}\right)=0\end{aligned} \tag{12}$$

The thermal bending deformations will be acquired by solving Eq. (12) using Galerkin method and least-squares iteration method.

In order to solve the static equation Eq. (12) and dynamic equation Eq. (9) conveniently, the following dimensionless quantities are defined.

$$\begin{aligned}&x=a\varsigma,\quad y=b\eta,\quad \lambda=a/b,\quad u^0=Uh^2/(12a),\quad v^0=Vh^2/(12a)\\ &w^0=Wh/(2\sqrt{3}),\quad \varphi_x=\varphi_\varsigma,\quad \varphi_y=\varphi_\eta,\quad q=QA_{11}h^3\Big/\left(24\sqrt{3}a^4\right)\end{aligned} \tag{13}$$

Eq. (12) can be written in the following dimensionless form:

$$\begin{aligned}
&U_{s,\varsigma\varsigma}+\delta_1U_{s,\eta\eta}+\delta_2V_{s,\varsigma\eta}+W_{s,\varsigma}\left(W_{s,\varsigma\varsigma}+\delta_1W_{s,\eta\eta}\right)+\delta_3W_{s,\eta}W_{s,\varsigma\eta}\\
&\quad+\delta_{44}N^T_{xx,\varsigma}+\delta_{45}N^T_{xy,\eta}=0U_{s,\varsigma\eta}+\delta_6V_{s,\varsigma\varsigma}+\delta_7V_{s,\eta\eta}+W_{s,\varsigma}W_{s,\varsigma\eta}\\
&\quad+W_{s,\eta}\left(\delta_8W_{s,\varsigma\varsigma}+\delta_9W_{s,\eta\eta}\right)+\delta_{46}N^T_{yy,\eta}+\delta_{47}N^T_{xy,\varsigma}\\
&=0W_{s,\varsigma}\begin{pmatrix}U_{s,\varsigma\varsigma}+\delta_1U_{s,\eta\eta}+\delta_2V_{s,\varsigma\eta}+W_{s,\varsigma}\left(W_{s,\varsigma\varsigma}+\delta_1W_{s,\eta\eta}\right)+\\ \delta_3W_{s,\eta}W_{s,\varsigma\eta}+\delta_{44}N^T_{xx,\varsigma}+\delta_{45}N^T_{xy,\eta}\end{pmatrix}\\
&\quad+W_{s,\eta}\begin{pmatrix}\delta_3U_{s,\varsigma\eta}+\delta_{28}V_{s,\varsigma\varsigma}+\delta_{22}V_{s,\eta\eta}+\delta_3W_{s,\varsigma}W_{s,\varsigma\eta}+\\ W_{s,\eta}\left(\delta_1W_{s,\varsigma\varsigma}+\delta_{29}W_{s,\eta\eta}\right)+\delta_{46}N^T_{yy,\eta}+\delta_{47}N^T_{xy,\varsigma}\end{pmatrix}\\
&\quad+W_{s,\varsigma\varsigma}\left(U_{s,\varsigma}+\delta_{16}W^2_{s,\varsigma}+\delta_{17}V_{s,\eta}+\delta_{18}W^2_{s,\eta}+\delta_{19}N^T_{xx}\right)\\
&\quad+W_{s,\eta\eta}\left(\delta_{20}U_{s,\varsigma}+\delta_{21}W^2_{s,\varsigma}+\delta_{22}V_{s,\eta}+\delta_{23}W^2_{s,\eta}+\delta_{24}N^T_{yy}\right)+\\
&\quad+W_{s,\varsigma\eta}\left(\delta_{25}U_{s,\eta}+\delta_{26}V_{s,\varsigma}+\delta_{25}W_{s,\varsigma}W_{s,\eta}+\delta_{27}N^T_{xy}\right)\\
&\quad+\delta_{12}\varphi_{\varsigma s,\varsigma}+\delta_{13}W_{s,\varsigma\varsigma}+\delta_{14}\varphi_{\eta s,\eta}+\delta_{15}W_{s,\eta\eta}=0\varphi_{\varsigma s,\varsigma\varsigma}\\
&\quad+\delta_{32}\varphi_{\varsigma s,\eta\eta}+\delta_{33}\varphi_{\eta s,\varsigma\eta}+\delta_{34}\varphi_{\varsigma s}+\delta_{35}W_{s,\varsigma}+\delta_{48}M^T_{xx,\varsigma}\\
&\quad+\delta_{49}M^T_{xy,\eta}=0\varphi_{\eta s,\eta\eta}+\delta_{38}\varphi_{\varsigma s,\varsigma\eta}+\delta_{39}\varphi_{\eta s,\varsigma\varsigma}+\delta_{41}\varphi_{\eta s}\\
&\quad+\delta_{40}W_{s,\eta}+\delta_{51}M^T_{yy,\eta}+\delta_{50}M^T_{xy,\varsigma}=0
\end{aligned}\tag{14}$$

The coefficients of Eq. (14) are given in Appendix.

The solutions of Eq. (14) are assumed as the following forms which satisfy the boundary conditions:

$$\begin{aligned}
U_s&=\sum_{m,n=1}^{M,N}u_{mn}I_m(\varsigma)J_n(\eta)\\
V_s&=\sum_{m,n=1}^{M,N}v_{mn}I_m(\varsigma)J_n(\eta)\\
W_s&=\sum_{m,n=1}^{M,N}w_{mn}R_m(\varsigma)S_n(\eta)\\
\varphi_{xs}&=\sum_{m,n=1}^{M,N}x_{mn}R'_m(\varsigma)S_n(\eta)\\
\varphi_{ys}&=\sum_{m,n=1}^{M,N}y_{mn}R_m(\varsigma)S'_n(\eta)
\end{aligned}\tag{15}$$

where u_{mn}, v_{mn}, w_{mn}, φ_{xmn}, φ_{ymn} are the undetermined coefficients irrelevant to time, and

$$\begin{aligned}
&I_m(\varsigma)=\sin m\pi\varsigma;\quad J_n(\eta)=\sin n\pi\eta\\
&R_m(\varsigma)=c_m(\cosh(\lambda_m\varsigma)-\cos(\lambda_m\varsigma))+d_m\sinh(\lambda_m\varsigma)+\sin(\lambda_m\varsigma)\\
&S_n(\eta)=c'_n(\cosh(\lambda'_n\eta)-\cos(\lambda'_n\eta))+d'_n\sinh(\lambda'_n\eta)+\sin(\lambda'_n\eta)
\end{aligned}\tag{16}$$

The coefficients d_m, c_m, λ_m, d'_n, c'_n, λ'_n are calculated according to the following equations:

$$\begin{aligned}
&d_m=-1;\quad c_m=\frac{\sin\lambda_m-\sinh\lambda_m}{\cos\lambda_m-\cosh\lambda_m};\quad 1-\cos\lambda_m\cosh\lambda_m=0\\
&d'_n=-1;\quad c'_n=\frac{\sin\lambda'_n-\sinh\lambda'_n}{\cos\lambda'_n-\cosh\lambda'_n};\quad 1-\cos\lambda'_n\cosh\lambda'_n=0
\end{aligned}\tag{17}$$

We then expand the membrane forces and bending moments due to temperature gradient in the double Fourier series as

$$\begin{Bmatrix}N^T_{xx}&M^T_{xx}\\N^T_{yy}&M^T_{yy}\\N^T_{xy}&M^T_{xy}\end{Bmatrix}=\sum_{m,n=1}^{M,N}\begin{Bmatrix}N^T_{xxmn}&M^T_{xxmn}\\N^T_{yymn}&M^T_{yymn}\\N^T_{xymn}&M^T_{xymn}\end{Bmatrix}R_m(\varsigma)S_n(\eta)\tag{18}$$

Substituting the displacement functions Eq. (15) into Eq. (14), using Galerkin method, multiplying the five equations in Eq. (14) by the weighted residuals I_kJ_l, I_kJ_l, R_kS_l, R'_kS_l, $R_kS'_l$, respectively, then carrying out the Simpson numerical integration, a set of nonlinear algebraic equations could be obtained. The static solutions are attained by solving the nonlinear algebraic equations with least-squares iteration method by MATLAB.

Vibrational responses could be obtained by solving Eq. (19) using Galerkin method and variable-step Runge–Kutta method. Equation (19) are the dimensionless forms of dynamic equation (9).

$$\begin{aligned}
&U_{,\varsigma\varsigma}+\delta_1U_{,\eta\eta}+\delta_2V_{,\varsigma\eta}+W_{,\varsigma}\left(W_{,\varsigma\varsigma}+\delta_1W_{,\eta\eta}\right)+\delta_3W_{,\eta}W_{,\varsigma\eta}+\delta_{44}N^T_{x,\varsigma}\\
&\quad+\delta_{45}N^T_{xy,\eta}=\delta_5U_{,tt}U_{,\varsigma\eta}+\delta_6V_{,\varsigma\varsigma}+\delta_7V_{,\eta\eta}+W_{,\varsigma}W_{,\varsigma\eta}\\
&\quad+W_{,\eta}\left(\delta_8W_{,\varsigma\varsigma}+\delta_9W_{,\eta\eta}\right)+\delta_{46}N^T_{y,\eta}+\delta_{47}N^T_{xy,\varsigma}\\
&=\delta_{11}V_{,tt}W_{,\varsigma}\begin{pmatrix}U_{,\varsigma\varsigma}+\delta_1U_{,\eta\eta}+\delta_2V_{,\varsigma\eta}+W_{,\varsigma}\left(W_{,\varsigma\varsigma}+\delta_1W_{,\eta\eta}\right)+\\ \delta_3W_{,\eta}W_{,\varsigma\eta}+\delta_{44}N^T_{x,\varsigma}+\delta_{45}N^T_{xy,\eta}\end{pmatrix}\\
&\quad+W_{,\eta}\begin{pmatrix}\delta_3U_{,\varsigma\eta}+\delta_{28}V_{,\varsigma\varsigma}+\delta_{22}V_{,\eta\eta}+\delta_3W_{,\varsigma}W_{,\varsigma\eta}+\\ W_{,\eta}\left(\delta_1W_{,\varsigma\varsigma}+\delta_{29}W_{,\eta\eta}\right)+\delta_{46}N^T_{y,\eta}+\delta_{47}N^T_{xy,\varsigma}\end{pmatrix}\\
&\quad+W_{,\varsigma\varsigma}\left(U_{,\varsigma}+\delta_{16}W^2_{,\varsigma}+\delta_{17}V_{,\eta}+\delta_{18}W^2_{,\eta}+\delta_{19}N^T_{x}\right)\\
&\quad+W_{,\eta\eta}\left(\delta_{20}U_{,\varsigma}+\delta_{21}W^2_{,\varsigma}+\delta_{22}V_{,\eta}+\delta_{23}W^2_{,\eta}+\delta_{24}N^T_{y}\right)\\
&\quad+W_{,\varsigma\eta}\left(\delta_{25}U_{,\eta}+\delta_{26}V_{,\varsigma}+\delta_{25}W_{,\varsigma}W_{,\eta}+\delta_{27}N^T_{xy}\right)+\delta_{12}\varphi_{\varsigma,\varsigma}\\
&\quad+\delta_{13}W_{,\varsigma\varsigma}+\delta_{14}\varphi_{\eta,\eta}+\delta_{15}W_{,\eta\eta}+Q=\delta_{31}W_{,tt}\varphi_{\varsigma,\varsigma\varsigma}+\delta_{32}\varphi_{\varsigma,\eta\eta}\\
&\quad+\delta_{33}\varphi_{\eta,\varsigma\eta}+\delta_{34}\varphi_{\varsigma}+\delta_{35}W_{,\varsigma}+\delta_{48}M^T_{x,\varsigma}+\delta_{49}M^T_{xy,\eta}=\delta_{37}\varphi_{\varsigma,tt}\varphi_{\eta,\eta\eta}\\
&\quad+\delta_{38}\varphi_{\varsigma,\varsigma\eta}+\delta_{39}\varphi_{\eta,\varsigma\varsigma}+\delta_{41}\varphi_{\eta}+\delta_{40}W_{,\eta}+\delta_{51}M^T_{y,\eta}+\delta_{50}M^T_{xy,\varsigma}\\
&=\delta_{43}\varphi_{\eta,tt}
\end{aligned}\tag{19}$$

The coefficients of Eq. (19) are given in Appendix.

The static displacements U_s, V_s, W_s, φ_{xs}, φ_{ys} have been solved by Eq. (14). According to the boundary conditions of all-edge clamped plate, the solutions of Eq. (19) are assumed as follows:

$$\begin{aligned}
U&=\sum_{m,n=1}^{M,N}(u_{mn}+u_{mn}(t))I_m(\varsigma)J_n(\eta)\\
V&=\sum_{m,n=1}^{M,N}(v_{mn}+v_{mn}(t))I_m(\varsigma)J_n(\eta)\\
W&=\sum_{m,n=1}^{M,N}(w_{mn}+w_{mn}(t))R_m(\varsigma)S_n(\eta)\\
\varphi_x&=\sum_{m,n=1}^{M,N}(x_{mn}+x_{mn}(t))R'_m(\varsigma)S_n(\eta)\\
\varphi_y&=\sum_{m,n=1}^{M,N}(y_{mn}+y_{mn}(t))R_m(\varsigma)S'_n(\eta)
\end{aligned}\tag{20}$$

where $u_{mn}(t)$, $v_{mn}(t)$, $w_{mn}(t)$, $\varphi_{xmn}(t)$, $\varphi_{ymn}(t)$ are the undetermined coefficients of dynamical displacements caused by the structural vibration. The coefficients of total displacement should be the sum of static coefficients and dynamical coefficients. Using Galerkin method, Eq. (19) could be transformed into a set of nonlinear ordinary differential equations. Taking the static displacement U_s, V_s, W_s, φ_{xs}, φ_{ys} caused by temperature gradient as the initial conditions of Eq. (19) as follows

$$\begin{aligned} U|_{t=0} &= U_s, & \left.\frac{dU}{dt}\right|_{t=0} &= 0 \\ V|_{t=0} &= V_s, & \left.\frac{dV}{dt}\right|_{t=0} &= 0 \\ W|_{t=0} &= W_s + W_{\max}, & \left.\frac{dW}{dt}\right|_{t=0} &= 0 \\ \varphi_x|_{t=0} &= \varphi_{xs}, & \left.\frac{d\varphi_x}{dt}\right|_{t=0} &= 0 \\ \varphi_y|_{t=0} &= \varphi_{ys}, & \left.\frac{d\varphi_y}{dt}\right|_{t=0} &= 0 \end{aligned} \tag{21}$$

where $W_{\max}$ is the dimensionless amplitude of the transverse displacement. Then, the dimensionless solutions of displacement can be obtained by using variable-step Runge–Kutta method for a time span numerically, which is a classical numerical method for solving differential equations implemented by MATLAB in this paper.

The responses can be transformed from time domain to frequency domain by FFT (Fast Fourier Transform).

$$F(\omega) = F[f(t)] = \int_{-\infty}^{\infty} f(t)e^{-i\omega t}dt \tag{22}$$

Resonant frequencies are obtained by the values of frequencies corresponding to resonant peaks.

Performing the Rayleigh integral, the sound pressure at the observation point (x_p, y_p, z_p) above the plate is acquired as

$$p(x_p, y_p, z_p, t) = \frac{j\omega\rho_0}{2\pi} e^{j\omega t} \int_{\Omega} \frac{\widetilde{v}(x,y,t)\cdot e^{-jkR}}{R} \mathrm{d}A \tag{23}$$

where ρ_0 is air density, $R = \sqrt{(x_p-x)^2 + (y_p-y)^2 + (z_p-z)^2}$ is the distance between the observation point (x_p, y_p, z_p) in acoustic field and the integration point, κ is the wave number which is evaluated by ω/c, c is the sound speed, $\widetilde{v}(x,y,t)$ is the first derivative of $w(x,y,t)$.

3. Validation

3.1. Validation for resonant frequency

In order to verify the correctness of present formula, resonant frequencies are compared with test result from Ref. [35], in which the test specimen is a 3 mm-thick aluminum plate with $0.3 \times 0.2\ \mathrm{m}^2$. The material properties are Young's modulus 65 GPa, Poisson's ratio 0.27, mass density 2810 kg m^{-3} and thermal expansion coefficient $2.3 \times 10^{-5}\ \mathrm{K}^{-1}$, respectively. The measured initial transverse deflection is 0.16 mm, which is due to the imperfection of the test specimen in Ref. [35].

To be more in accord with the actual geometric shape of the plate, the initial transverse deflections should be added to the present theoretical calculation as described below. In formulation of Section 2, the mid-plane temperature T_0 induces thermal expansion or contraction stresses, while initial transverse deflections are induced by thermal bending moment due to temperature gradient τ. Initial transverse deflection is added in a similar way which is to add the temperature gradient load $\Delta T_i = \tau_i z$ to the formulation. Because the mid-plane temperature is not included in ΔT_i and there will not be thermal expansion or contraction stresses, only initial transverse deflection will be induced.

Assigning the initial transverse deflection to be $w_s^0(x,y)$ in Eq. (3), and then performing the same formulations with Section 2, resonant frequencies will be obtained by Eq. (19) using variable-step Runge–Kutta method and FFT (Fast Fourier Transform). It can be seen from Fig. 2 that the resonant frequencies calculated in the present work agree well with FEM (Nastran) in Ref. [35].

As mentioned above, initial transverse deflection is added in the present theoretical calculation for imperfect of the test specimen. In the finite element analysis, initial imperfection is also to be considered. Assuming that the node coordinate is $\mathbf{X_i^0}(x,y,z)$ for a flat plate, modifying the FEM model of the flat plate, making it with the initial transverse deflection $\boldsymbol{\delta_i}(x,y,z)$, then the flat plate turns into a curve plate with initial geometrical imperfections, of which node coordinate turns into $\mathbf{X_i^0}(x,y,z) = \mathbf{X_i^0}(x,y,z) + \boldsymbol{\delta_i}(x,y,z)$. It is different from the previous flat plate that both geometrical imperfections and thermal stress are considered in the finite element analysis [35]. Besides, the deviation in Fig. 2 between the present work and the experiment results is for two reasons. One is explained in details in Ref. [35] that the thermal expansion of the experimental frame will release some of the thermal stresses and thermal deflection of the test plate. Therefore, in the present theoretical calculations, we reduce the thermal stress 10%, 20%, 30% corresponding to 'off stress 10%', 'off stress 20%', 'off stress 30%' respectively in Fig. 3 to simulate that experimental frame releases some of the thermal stresses. The result shows that present theoretical results get closer to the experiment results with the decrease of thermal stresses, and thereby support the reason that the experimental frame releases part of the thermal stresses and thermal deflection of the test plate. The other reason is supposed that Young's modulus is dependent on temperature, which is not focused in present work. To check whether it is for this, temperature-dependent Young's modulus and thermal expansion

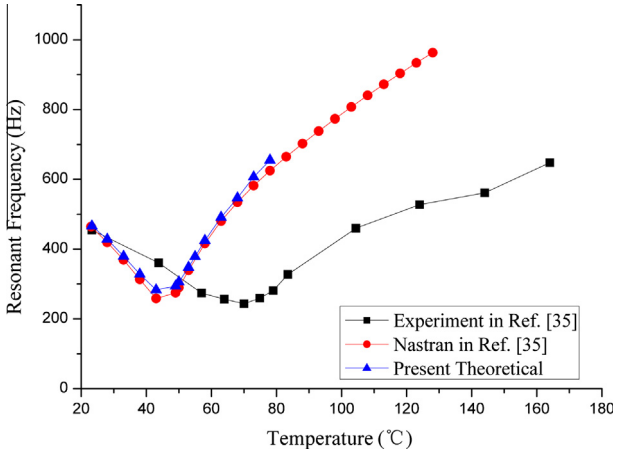

Fig. 2. Comparison of resonant frequency.

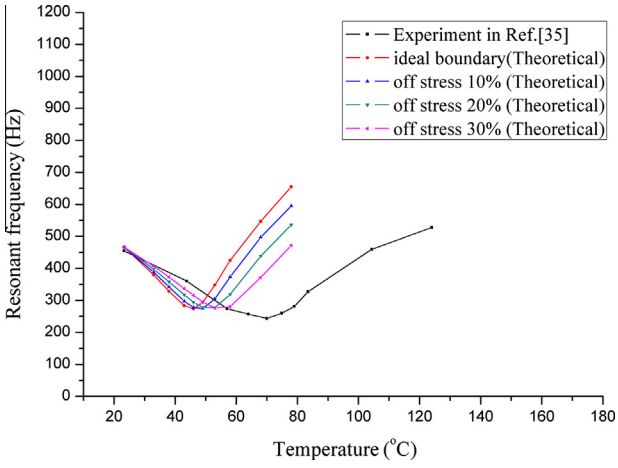

Fig. 3. Comparison of resonant frequency with different release of thermal stresses.

Table 1
Temperature-dependent Young's modulus and thermal expansion coefficient of aluminum.

Young's modulus (MPa)	Thermal expansion (/K)
$65144 + 73.432T - 0.1618T^2$	$2 \times 10^{-5} + 6 \times 10^{-9}T + 3 \times 10^{-12}T^2 + 10^{-14}T^3$

coefficient of aluminum are shown in Table 1 [36]. Considering temperature-dependent and temperature-independent Young's modulus in present theoretical calculations, resonant frequencies are compared with experiment results. It can be seen from Fig. 4 that there is no obvious change in value and tendency for the results between temperature-dependent and temperature-independent Young's modulus compared with experiment results. It indicates that temperature-dependent Young's modulus is not a main cause of the deviation in Fig. 2. Also, for the present temperatures range, temperature-dependent Young's modulus exerts very little influence on the resonant frequency. Consequently, it's reasonable and acceptable that present work considers temperature-independent Young's modulus.

So far, the present work theoretically explains why the lowest point (buckling occurring) of the experimental curve of resonant frequencies for thermal structure is shifting up away from the horizontal axis (see Fig. 2).

3.2. Validation for response

Numerical simulation is performed to validate the dynamic response of the present study by the finite element software ABAQUS. An all-edge clamped rectangular symmetric 3-layer plate is considered and simulated using $80 \times 60 \times 7$ 3D solid elements. The material properties of the plate with dimensions $0.4 \times 0.3 \times 0.007\ m^3$ are given in Table 2. A harmonic excitation with amplitude of 20,000 N and frequency of 50 Hz is applied at the center of the plate. The mid-plane temperature is 40 °C. The comparisons of displacement responses at the center of the plate under different temperature gradients 1 °C mm^{-1} and 4 °C mm^{-1} are shown in Figs. 5 and 6, respectively. According to above mentioned in Section 3.1, it could be seen that initial thermal deformation and thermal stress have to be considered together in simulation of the dynamical response for thermal structure. The solving processes by ABAQUS consist of two steps: (1) Static General; (2) Dynamic Implicit. Initial thermal deformation and thermal stress would be induced by exerting temperature gradient to the finite element model in static analysis process step 1, then taking the end state of step 1 as the initial state of dynamical analysis process step 2, the solutions of responses could be obtained by implicit reduction method in step 2.

It can be observed the present results match well with the results calculated by ABAQUS on the whole, although there is a little deviation because the selected displacement functions are

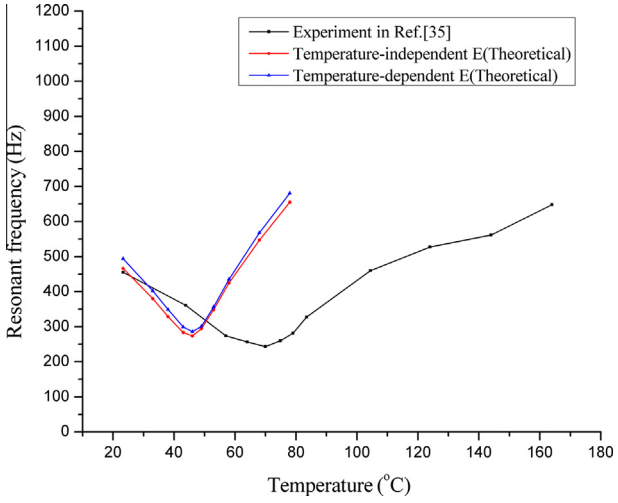

Fig. 4. Comparison of resonant frequency with temperature-dependent and temperature-independent material properties.

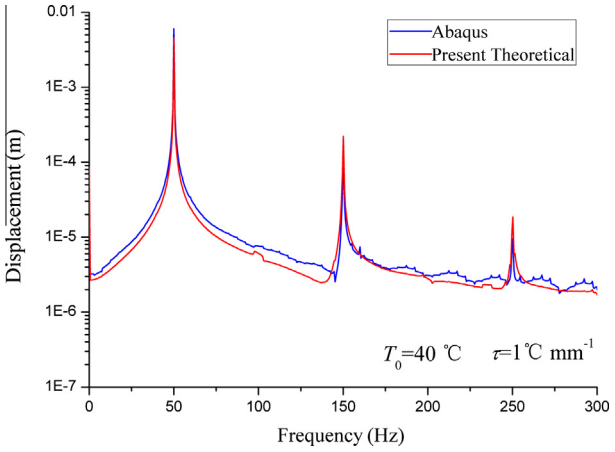

Fig. 5. Comparison of displacement response, $\tau = 1$ °C mm^{-1}.

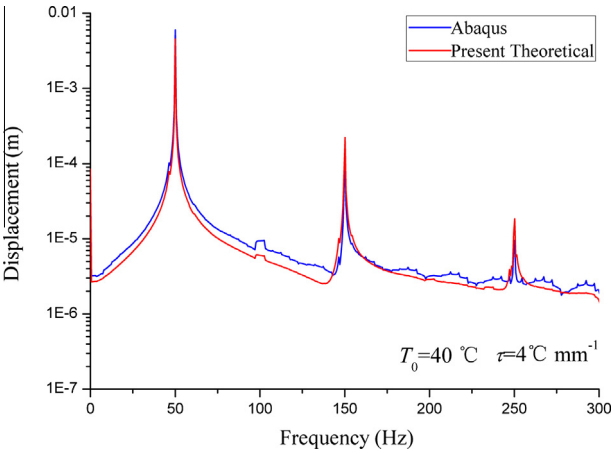

Fig. 6. Comparison of displacement response, $\tau = 4$ °C mm^{-1}.

Table 2
Material properties and parameters for each layer.

Density (kg m^{-3})	Young's modulus (GPa)	Poisson's ratio	Thermal expansion	Thickness (m)
4500	110	0.33	1e−5	2e−3
2700	70	0.3	2.3e−5	3e−3
4500	110	0.33	1e−5	2e−3

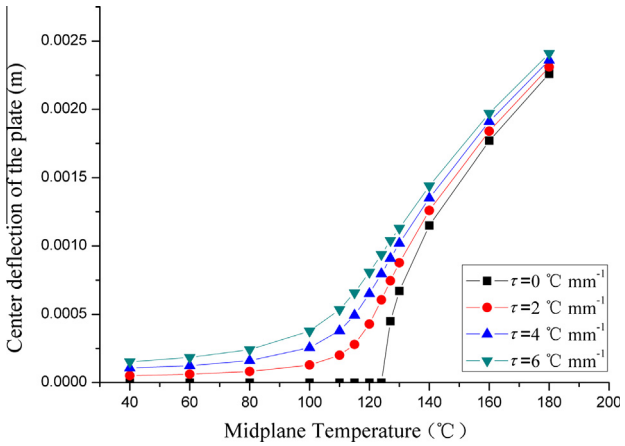

Fig. 7. Center deflection of plate under different temperature gradients.

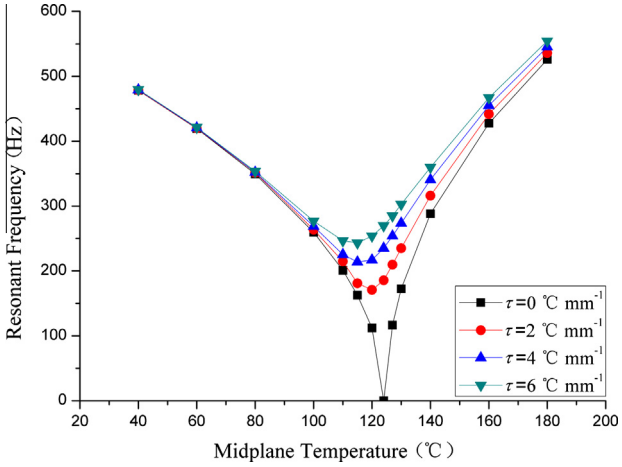

Fig. 8. Resonant frequency under different temperature gradients.

approximate solutions which are not accurate enough to express the displacement. The present approach for vibration responses can still be considered valid.

4. Results and discussions

Some cases are solved to study temperature gradient effect on the laminated plates. Resonant frequencies, vibrational and acoustic responses are calculated with different temperature gradients and initial deflections. Material properties and dimensions of the laminated plate are identical with Section 3.2.

4.1. Different temperature gradients

Initial deflections are acquired by solving Eq. (12) using Galerkin method and least-squares iteration method. Resonant frequencies are obtained by Eq. (19) using variable-step Runge–Kutta method and FFT (Fast Fourier Transform). To be closer to the actual stiffness, the dimensionless amplitude of free vibration is given a small value 1e−5 as the initial disturbance. It can be observed that the deflections in Fig. 7 increase as the temperature gradient increases. This is because thermal bending moment increases with temperature gradient increasing, which leads to the increasing of the initial deflections of the laminated plate. Fig. 8 shows that the resonant frequency increases as the temperature gradient increases. This is due to that initial deflections caused by temperature gradient intensify the stiffness of the structure. Accordingly, resonant frequency is enhanced.

In Fig. 8, the mid-plane temperature at which resonant frequency drops to the lowest is defined as critical mid-plane temperature. The resonant frequency at the critical mid-plane temperature for 0 °C mm^{-1} is near to 0 Hz for critical mid-plane temperature is near to critical buckling temperature. However, the resonant frequencies at the critical mid-plane temperature for 2 °C mm^{-1}, 4 °C mm^{-1}, 6 °C mm^{-1} are higher than 0 Hz. This is because the temperature gradients induce the transverse deflections which contribute to geometric stiffness.

Also, it is worth noting that the critical mid-plane temperature moves toward lower temperature as temperature gradient increases. The reason is before the critical mid-plane temperature, softening effect on the laminated plate is induced by the thermal stress due to the mid-plane temperature, and stiffening effect is induced by deformation due to temperature gradient, softening effect is greater than stiffening effect, the resonant frequency gets decreased. At the critical mid-plane temperature, softening effect is equal to stiffening effect and the resonant frequency reaches the minimum. After the critical mid-plane temperature, stiffening effect increases because of post-buckling deflections. Softening effect is smaller than stiffening effect, the resonant frequency gets increased. For a greater temperature gradient makes greater stiffening effect, softening effect at lower mid-plane temperature

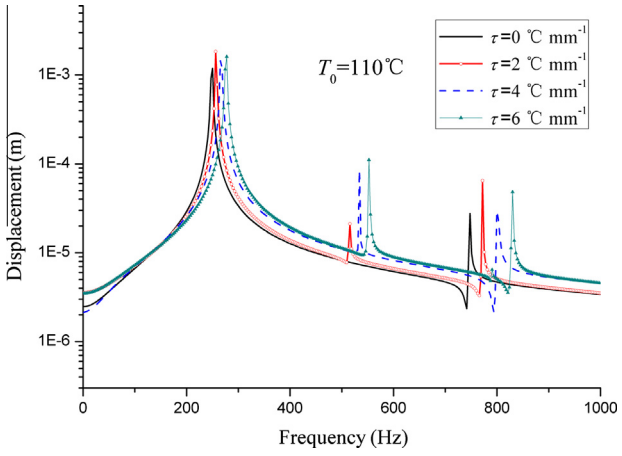

Fig. 9. Displacement responses under different temperature gradients.

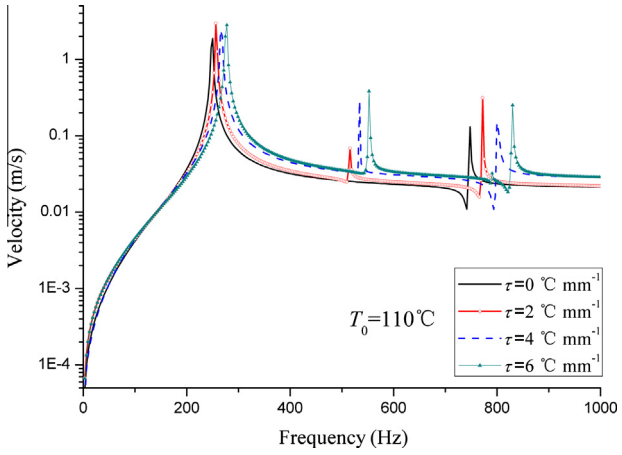

Fig. 10. Velocity responses under different temperature gradients.

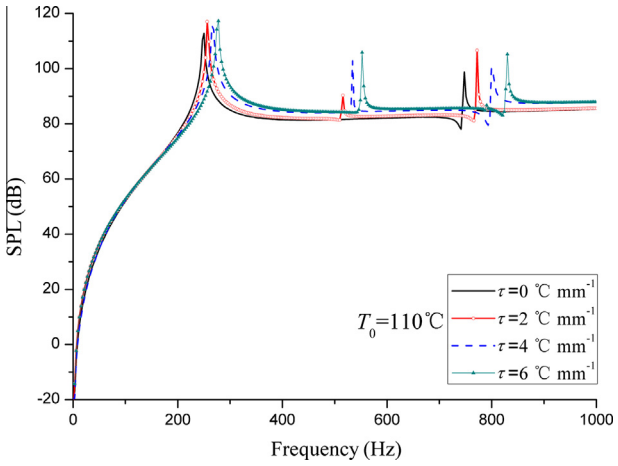

Fig. 11. Sound pressure level under different temperature gradients.

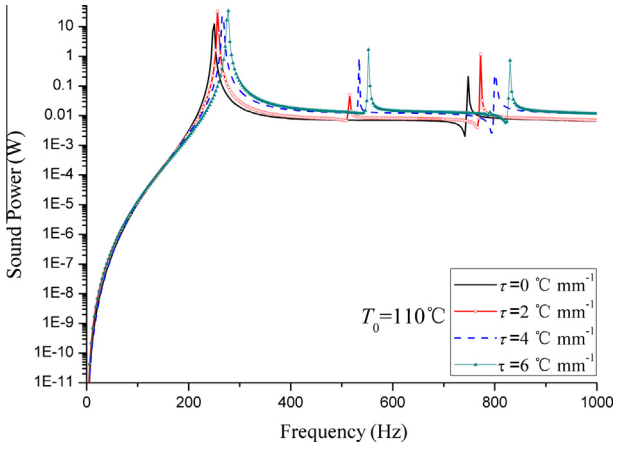

Fig. 12. Sound Power under different temperature gradients.

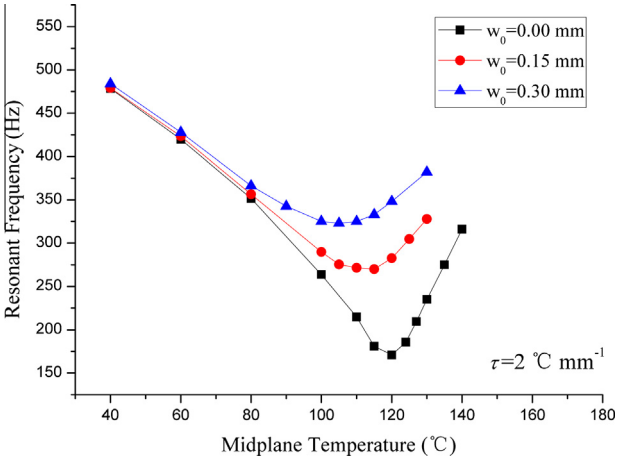

Fig. 13. Resonant frequency with different initial deflections.

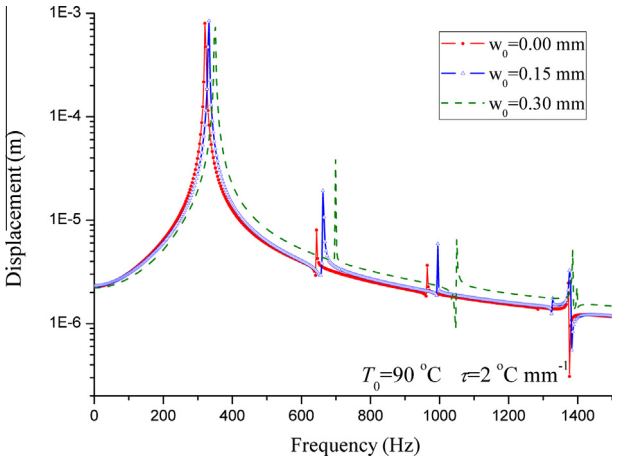

Fig. 14. Displacement response with different initial deflections.

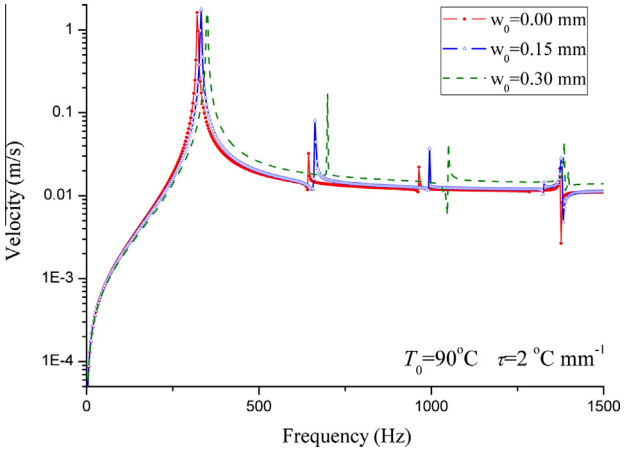

Fig. 15. Velocity response with different initial deflections.

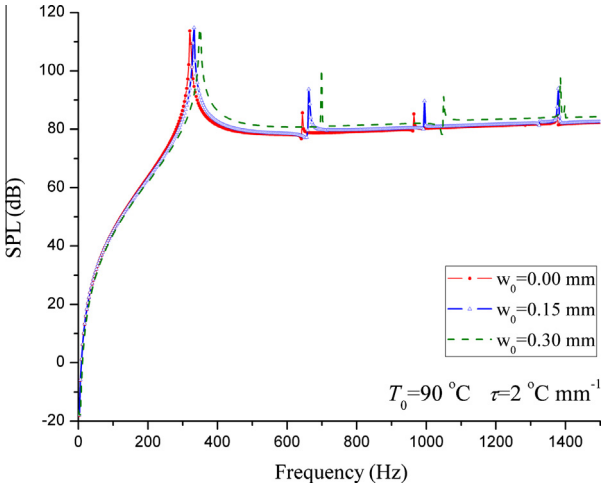

Fig. 16. Sound pressure level response with different initial deflections.

reaches balance. The critical mid-plane temperature moves toward lower temperature as temperature gradient increases.

The Figs. 9–12 show frequency response curves of displacement, velocity, sound pressure level and sound power of the laminated plate under different temperature gradients. The mid-plane temperature is 110 °C.

The dimensionless amplitude of free vibration is 0.5. The displacement response, velocity response are calculated at the point (0.12 m, 0.9 m, 0 m) and the sound pressure level response is calculated at the point (0.12 m, 0.9 m, 0.3 m). It can be seen that the resonant frequencies move towards high frequencies with

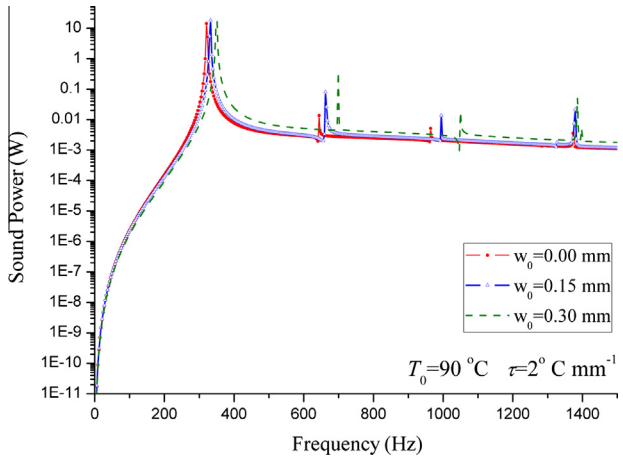

Fig. 17. Sound power with different initial deflections.

the temperature gradients increasing. Because the temperature gradient induces the thermal bending moment, which leads to the deformation of laminated plate. The geometric deformation makes the stiffness of structures enhanced. Accordingly, the resonant frequency increases.

4.2. Different initial deflections

From the analysis in the Section 4.1, it can be found that initial deformation induced by temperature gradient is significant to the vibration and acoustic characteristics. Besides temperature gradient, there are many factors contributing to the initial deformation of plates, such as processing defect.

Initial deflection w_0 induced by assuming a temperature load $\Delta T_i = \tau_i z$ is added to the Eq. (3) as described in Section 3.1 in details. Then it is solved by Eq. (12) with Galerkin method and least-squares iteration method. Vibrational and acoustic responses are obtained by the formulations in Section 2. The dimensionless amplitude of free vibration is 0.3. The responses are calculated at the same points with Section 4.1. As shown in Figs. 13–17, the effect of initial deflections due to other factors on the vibration and acoustic characteristics is found similar to that caused by temperature gradient.

5. Conclusion

The effects of temperature gradient on the dynamic characteristics and responses for a laminated plate are studied in this paper. Based on the first order shear deformation theory and von Karman nonlinear strain displacement relationship, the governing equations are established considering the temperature gradient along the thickness. Semi-analytical solutions of resonant frequency, displacement, velocity response and sound pressure level and sound power are obtained by using variable-step Runge–Kutta method and Rayleigh integral. Simple experiment cases are utilized to validate the present solutions, and the present work theoretically explains why the lowest point (buckling occurring) of the experimental curve of resonant frequencies for thermal structure is shifting up away from the horizontal axis. It also means that initial thermal deformation and thermal stress have to be considered together in simulation of the dynamical response for thermal structure.

According to the results, there is similar influence on vibrational and acoustic responses of temperature gradients and initial deflections. As temperature gradient (or initial deflection) increases, the resonant frequency increases, for temperature gradient (or initial deflection) leads to stiffening effect on the plate, while the critical mid-plane temperature moves toward lower mid-plane temperature; the response peaks move toward higher frequency with the increase in temperature gradient (or initial deflection).

Acknowledgements

This work is supported by the National Natural Science Foundation of China (Grant Nos. 11321062 and 11472206), National Basic Research Program of China (No. 2013CB035704) and China Postdoctoral Science Foundation (No. 2015M582641).

Appendix A

$$\delta_1 = A_{66}\lambda^2/A_{11},\ \delta_2 = (A_{12}+A_{66})\lambda/A_{11},\ \delta_3 = (A_{12}+A_{66})\lambda^2/A_{11},$$
$$\delta_4 = -12a^3/(A_{11}h^2),\ \delta_5 = R_0a^2/A_{11},\ \delta_6 = A_{66}/[(A_{12}+A_{66})\lambda],$$
$$\delta_7 = A_{22}\lambda/(A_{12}+A_{66}),\ \delta_8 = A_{66}/(A_{12}+A_{66}),\ \delta_9 = A_{22}\lambda^2/(A_{12}+A_{66}),$$
$$\delta_{10} = -12a^2b/[(A_{12}+A_{66})h^2],\ \delta_{11} = R_0ab/(A_{12}+A_{66}),$$
$$\delta_{12} = 24\sqrt{3}a^3A_{55}/(A_{11}h^3),$$
$$\delta_{13} = 12a^2A_{55}/(A_{11}h^2),\ \delta_{14} = 24\sqrt{3}a^3A_{44}\lambda/(A_{11}h^3),$$
$$\delta_{15} = 12a^2\lambda^2A_{44}/(A_{11}h^2),$$
$$\delta_{16} = 1/2,\ \delta_{17} = A_{12}\lambda/A_{11},\ \delta_{18} = A_{12}\lambda^2/(2A_{11}),$$
$$\delta_{19} = -12a^2/(A_{11}h^2),\ \delta_{20} = A_{12}\lambda^2/A_{11},\ \delta_{21} = A_{12}\lambda^2/(2A_{11}),$$
$$\delta_{22} = A_{22}\lambda^3/A_{11},\ \delta_{23} = A_{22}\lambda^4/(2A_{11}),\ \delta_{24} = -12a^2\lambda^2/(A_{11}h^2),$$
$$\delta_{25} = 2A_{66}\lambda^2/A_{11},\ \delta_{26} = 2A_{66}\lambda/A_{11},\ \delta_{27} = -24a^2\lambda/(A_{11}h^2),$$
$$\delta_{28} = A_{66}\lambda/A_{11},\ \delta_{29} = A_{22}\lambda^4/A_{11},\ \delta_{30} = -12a^3\lambda/(A_{11}h^2),$$
$$\delta_{31} = 12R_0a^4/(A_{11}h^2),\ \delta_{32} = D_{66}\lambda^2/D_{11},\ \delta_{33} = (D_{12}+D_{66})\lambda/D_{11},$$
$$\delta_{34} = -A_{55}a^2/D_{11},\ \delta_{35} = -A_{55}ah/(2\sqrt{3}D_{11}),\ \delta_{36} = -a^2/D_{11},$$
$$\delta_{37} = R_2a^2/D_{11},\ \delta_{38} = (D_{21}+D_{66})/(D_{22}\lambda),\ \delta_{39} = D_{66}/(D_{22}\lambda^2),$$
$$\delta_{40} = -A_{44}bh/(2\sqrt{3}D_{22}),\ \delta_{41} = -A_{44}b^2/D_{22},\ \delta_{42} = -b^2/D_{22},$$
$$\delta_{43} = R_2b^2/D_{22},\ \delta_{44} = \delta_4/a,\ \delta_{45} = \delta_4/b,$$
$$\delta_{46} = \delta_{10}/b,\ \delta_{47} = \delta_{10}/a,\ \delta_{48} = \delta_{36}/a,$$
$$\delta_{49} = \delta_{36}/b;\ \delta_{50} = \delta_{42}/a,\ \delta_{51} = \delta_{42}/b$$

References

[1] Jeyaraj P, Padmanabhan C, Ganesan N. Vibration and acoustic response of an isotropic plate in a thermal environment. J Vib Acoust 2008;130(5):301–6. http://dx.doi.org/10.1115/1.2948387.
[2] Jeyaraj P, Ganesan N, Padmanabhan C. Vibration and acoustic response of a composite plate with inherent material damping in a thermal environment. J Sound Vib 2009;320(1–2):322–38. http://dx.doi.org/10.1016/j.jsv.2008.08.013.
[3] Yang J, Shen HS. Vibration characteristics and transient response of shear-deformable functionally grade plates in thermal environment. J Sound Vib 2002;255(3):579–602. http://dx.doi.org/10.1006/jsvi.2001.4161.
[4] Jha DK, Kant T, Singh RK. Free vibration response of functionally graded thick plates with shear and normal deformations effects. Compos Struct 2013;96(4):799–823. http://dx.doi.org/10.1016/j.compstruct.2012.09.034.
[5] Vangipuram P, Ganesan N. Buckling and vibration of rectangular composite viscoelastic sandwich plates under thermal loads. Compos Struct 2007;77(4):419–29. http://dx.doi.org/10.1016/j.compstruct.2005.07.012.
[6] Pradeep V, Ganesan N. Thermal buckling and vibration behavior of multi-layer rectangular viscoelastic sandwich plates. J Sound Vib 2008;310(1–2):169–83. http://dx.doi.org/10.1016/j.jsv.2007.07.083.
[7] Geng Q, Li YM. Analysis of dynamic and acoustic radiation characters for a flat plate under thermal environments. Int J Appl Mech 2012;4(3):16. http://dx.doi.org/10.1142/S1758825112500287.
[8] Geng Q, Li YM. Solutions of dynamic and acoustic responses of a clamped rectangular plate in thermal environments. J Vib Control 2014. http://dx.doi.org/10.1177/1077546314543730. Prepublished July 25.
[9] Geng Q, Li H, Li YM. Dynamic and acoustic response of a clamped rectangular plate in thermal environments: experiment and numerical simulation. J Acoust Soc Am 2014;135(5):2674–82. http://dx.doi.org/10.1121/1.4870483.

[10] Liu Y, Li Y. Vibration and acoustic response of rectangular sandwich plate under thermal environment. Shock Vib 2013;20(5):1011–30. http://dx.doi.org/10.3233/SAV-130801.
[11] Li W, Li YM. Vibration and sound radiation of an asymmetric laminated rectangular plate in thermal environments. Acta Mech Solida Sin 2015;28(1):11–22. http://dx.doi.org/10.1016/S0894-9166(15)60011-8.
[12] Li XY, Yu KP. Vibration and acoustic responses of composite and sandwich panelsunder thermal environment. Compos Struct 2015;131:1040–9.
[13] Zhang XL, Yu KP, Bai YH, Zhao R. Thermal vibration characteristics of fiber-reinforced mullite sandwich structure with ceramic foams core. Compos Struct 2015;131:99–106.
[14] Natarajan S, Deogekar PS, Manickam G, Belouettar S. Hygrothermal effects on the free vibration and buckling of laminated composites with cutouts. Compos Struct 2014;108(1):848–55. http://dx.doi.org/10.1016/j.compstruct.2013.10.009.
[15] Panda HS, Sahu SK, Parhi PK. Hygrothermal effects on free vibration of delaminated woven fiber composite plates – numerical and experimental results. Compos Struct 2013;96(4):502–13. http://dx.doi.org/10.1016/j.compstruct.2012.08.057.
[16] Rath MK, Sahu SK. Vibration of woven fiber laminated composite plates in hygrothermal environment. J Vib Control 2012;18(13):1957–70. http://dx.doi.org/10.1177/1077546311428638.
[17] Itishree M, Shishir KS. An experimental approach to free vibration response of woven fiber composite plates under free-free boundary condition. Int J Adv Technol Civil Eng 2012;1(2):2231–5721.
[18] Dhotarad MS, Ganesan N. Vibration analysis of a rectangular plate subjected to a thermal gradient. J Sound Vib 1978;60(4):481–97. http://dx.doi.org/10.1016/S0022-460X(78)80087-X.
[19] Dhotarad MS, Ganesan N. Influence of thermal gradient on natural frequency of rectangular plate vibration. Nucl Eng Des 1979;52(1):71–81. http://dx.doi.org/10.1016/0029-5493(79)90009-8.
[20] Gupta AK, Kumar L. Thermal effect on vibration of non-homogenous visco-elastic rectangular plate of linearly varying thickness. Meccanica 2008;43(1):47–54. http://dx.doi.org/10.1007/s11012-007-9093-3.
[21] Fauconneau G, Marangoni RD. Effect of a thermal gradient on the natural frequencies of a rectangular plate. Int J Mech Sci 1970;12(2):113–22. http://dx.doi.org/10.1016/0020-7403(70)90011-1.
[22] Chen CS, Chen CW, Chen WR, Chang YC. Thermally induced vibration and stability of laminated composite plates with temperature dependent properties. Meccanica 2013;48(9):2311–23. http://dx.doi.org/10.1007/s11012-013-9750-7.
[23] Girish J, Ramachandra LS. Thermal postbuckled vibrations of symmetrically laminated composite plates with initial geometric imperfections. J Sound Vib 2005;282(3–5):1137–53. http://dx.doi.org/10.1016/j.jsv.2004.04.005.
[24] Park JS, Kim JH. Thermal postbuckling and vibration analyses of functionally graded plates. J Sound Vib 2006;289(1–2):77–93. http://dx.doi.org/10.1016/j.jsv.2005.01.031.
[25] Shooshtari A, Razavi S. A closed form solution for linear and nonlinear free vibrations of composite and fiber metal laminated rectangular plates. Compos Struct 2010;92(11):2663–75. http://dx.doi.org/10.1016/j.compstruct.2010.04.001.
[26] Amabili M. Nonlinear vibrations of rectangular plates with different boundary conditions: theory and experiments. Comput Struct 2004;82(31–32):2587–605. http://dx.doi.org/10.1016/j.compstruc.2004.03.077.
[27] Amabili M. Theory and experiments for large-amplitude vibrations of rectangular plates with geometric imperfections. J Sound Vib 2006;291(3–5):539–65. http://dx.doi.org/10.1016/j.jsv.2005.06.007.
[28] Bhimaraddi A, Chandrashekhara K. Nonlinear vibrations of heated antisymmetric angle-ply laminated plates. Int J Solids Struct 1993;30(9):1255–68. http://dx.doi.org/10.1016/0020-7683(93)90015-Y.
[29] Chen CS, Hwang JR, Doong JL. Nonlinear vibration of an initially stressed plate based on a modified plate theory. Int J Solids Struct 2001;38(46–47):8563–83. http://dx.doi.org/10.1016/S0020-7683(00)00226-2.
[30] Shen HS. Nonlinear bending response of functionally graded plates subjected to transverse loads and in thermal environments. Int J Mech Sci 2002;44(3):561–84. http://dx.doi.org/10.1016/S0020-7403(01)00103-5.
[31] Huang XL, Shen HS. Nonlinear vibration and dynamic response of functionally graded plates in thermal environments. Int J Solids Struct 2009;41(9–10):2403–7. http://dx.doi.org/10.1016/j.ijsolstr.2003.11.012.
[32] Murphy KD, Vurgin LN, Rizzi SA. The effect of thermal prestress on the free vibration characteristics of clamped rectangular plates theory and experiment. J Vib Acoust 1997;119(2):243–9. http://dx.doi.org/10.1115/1.2889710.
[33] Li SR, Zhou YH. Nonlinear vibration and thermal buckling of an orthotropic annular plate with a centric rigid mass. J Sound Vib 2002;251(1):141–52. http://dx.doi.org/10.1006/jsvi.2001.3987.
[34] Li SR, Zhou YH. Nonlinear Vibration of heated orthotropic annular plates with immovably hinged edges. J Therm Stresses 2003;26(7):691–700. http://dx.doi.org/10.1080/713855995.
[35] Geng Q, Wang D, Liu Y, Li YM. Experimental and numerical investigations on dynamic and acoustic responses of a thermal post-buckled plate. Sci China Technol Sci 2015;25(8):1414–24. http://dx.doi.org/10.1007/s11431-015-5838-8.
[36] Khan KA. A multiscale model for coupled heat conduction and deformations of viscoelastic composites [Ph. D. thesis], Texas A&M University; 2011.